Effects of substrate stiffness and actomyosin contractility on coupling between force transmission and vinculin–paxillin recruitment at single focal adhesions

Dennis W. Zhou[a], Ted T. Lee[b], Shinuo Weng[c], Jianping Fu[c,d], and Andrés J. García[b,*]
[a]Wallace H. Coulter Department of Biomedical Engineering, Interdisciplinary Bioengineering Graduate Program, and [b]Woodruff School of Mechanical Engineering, Petit Institute for Bioengineering and Bioscience, Georgia Institute of Technology, Atlanta, GA 30332; [c]Department of Mechanical Engineering and [d]Department of Biomedical Engineering and Department of Cell and Developmental Biology, University of Michigan, Ann Arbor, MI 48109

ABSTRACT **Focal adhesions (FAs) regulate force transfer between the cytoskeleton and ECM–integrin complexes. We previously showed that vinculin regulates force transmission at FAs. Vinculin residence time in FAs correlated with applied force, supporting a mechanosensitive model in which forces stabilize vinculin's active conformation to promote force transfer. In the present study, we examined the relationship between traction force and vinculin–paxillin localization to single FAs in the context of substrate stiffness and actomyosin contractility. We found that vinculin and paxillin FA area did not correlate with traction force magnitudes at single FAs, and this was consistent across different ECM stiffness and cytoskeletal tension states. However, vinculin residence time at FAs varied linearly with applied force for stiff substrates, and this was disrupted on soft substrates and after contractility inhibition. In contrast, paxillin residence time at FAs was independent of local applied force and substrate stiffness. Paxillin recruitment and residence time at FAs, however, were dependent on cytoskeletal contractility on lower substrate stiffness values. Finally, substrate stiffness and cytoskeletal contractility regulated whether vinculin and paxillin turnover dynamics are correlated to each other at single FAs. This analysis sheds new insights on the coupling among force, substrate stiffness, and FA dynamics.**

Monitoring Editor
Valerie Marie Weaver
University of California, San Francisco

Received: Feb 22, 2017
Revised: Mar 31, 2017
Accepted: Apr 27, 2017

INTRODUCTION

Cell adhesion to the extracellular matrix (ECM) is regulated by integrin receptors (Humphries *et al.*, 2006). After binding to ECM proteins, integrin clustering occurs to form focal adhesion (FA) complexes, which contain structural proteins that link the cell cytoskeleton to the ECM and signaling effectors that regulate cell division, migration, and differentiation (Mitra *et al.*, 2005; Provenzano and Keely, 2011; Kuroda *et al.*, 2017). FAs provide cell anchorage by mechanically linking ECM proteins to the cytoskeleton (Humphries *et al.*, 2006, 2009) and transmitting adhesive forces that drive signaling, proliferation, and tissue morphogenesis (Provenzano and Keely, 2011; Yang *et al.*, 2011; Heisenberg and Bellaiche, 2013). Actomyosin contractility plays a critical role in generating cell adhesive forces (Tan *et al.*, 2003; Dumbauld *et al.*, 2010; Pasapera *et al.*, 2010) and influences FA composition and size (Chrzanowska-Wodnicka and Burridge, 1996; Giannone *et al.*, 2007). Single-molecule experiments support a model for force-induced talin unfolding, which exposes cryptic binding sites for vinculin (del Rio *et al.*, 2009). Furthermore, actomyosin contractility controls the recruitment of several FA proteins, such as vinculin and focal adhesion kinase (FAK; Pasapera *et al.*, 2010).

Mechanosensitive responses to ECM stiffness influence diverse cell behaviors, such as cell fate commitment, migration, spreading, and FA assembly (Yeung *et al.*, 2005; Engler *et al.*, 2006). Previous

This article was published online ahead of print in MBoC in Press (http://www.molbiolcell.org/cgi/doi/10.1091/mbc.E17-02-0116) on May 3, 2017.
*Address correspondence to: Andrés J. García (andres.garcia@me.gatech.edu).
Abbreviations used: ECM, extracellular matrix; FA, focal adhesion; FRAP, fluorescence recovery after photobleaching.

analyses revealed that stiffer substrates promote increased cell spreading and traction force generation (Lo *et al.*, 2000) and larger FAs (Pelham and Wang, 1997). FAs have also been implicated as principal sites for stiffness mechanosensing through modules such as a FAK-phospho-paxillin-vinculin signaling axis (Plotnikov *et al.*, 2012), talin isoforms (Austen *et al.*, 2015), and vinculin through its head–tail interactions (Liu *et al.*, 2016). Furthermore, localization of certain FA proteins, such as vinculin, is significantly influenced by substrate stiffness, whereas localization of other FA proteins, including paxillin, is relatively insensitive to substrate stiffness (Pasapera *et al.*, 2010).

Although previous studies examined the effects of substrate stiffness and cytoskeletal tension on FA assembly, it is unclear how FA assembly is related to local adhesive force generation at the single-FA level. In particular, the relationship between traction force and FA assembly is poorly understood. Both positive correlation (Balaban *et al.*, 2001; Tan *et al.*, 2003; Weng *et al.*, 2016) and inverse correlation between force and FA size for FAs along the leading edge of cells (Beningo *et al.*, 2001) have been reported. Furthermore, others have reported lower forces during FA disassembly, whereas increases in force are correlated with FA assembly (Grashoff *et al.*, 2010). Indeed, coupling between FA size and traction force is limited to the initial period during FA growth, where, in the absence of growth history, FA size is a poor predictor of traction force (Stricker *et al.*, 2011). Regardless of these conflicting results, it is well accepted that applied forces regulate FA size by modulating FA kinetics (Wolfenson *et al.*, 2011; Dumbauld *et al.*, 2013).

Vinculin regulates force transmission between the cell and its ECM (Dumbauld *et al.*, 2013). Vinculin consists of a globular head domain (V_H) that is linked to a tail domain (V_T) by a proline-rich strap (Ziegler *et al.*, 2006). The V_H domain contains binding sites for talin and α-actinin (Chen *et al.*, 2005; Chen *et al.*, 2006). The V_T domain includes binding sites for actin, phosphatidylinositol 4,5-biphosphate (Palmer *et al.*, 2009), and paxillin (Subauste *et al.*, 2004). Furthermore, the proline-rich strap contains binding sites for vasodilator-stimulated phosphoprotein (Brindle *et al.*, 1996) and actin-related protein 2/3 (DeMali *et al.*, 2002). Vinculin displays high-affinity head–tail binding, which leads to autoinhibition and regulates vinculin's interactions with its binding partners at the head and tail domains (Johnson and Craig, 1995; Cohen *et al.*, 2005). Vinculin activation is hypothesized to occur at FAs upon simultaneous binding between talin and actin (Chen *et al.*, 2005, 2006; Case *et al.*, 2015). Moreover, reports show that actomyosin contractility and substrate stiffness influence vinculin recruitment to FAs (Pasapera *et al.*, 2010; Wolfenson *et al.*, 2011; Yamashita *et al.*, 2014; Kuroda *et al.*, 2017).

Paxillin is a multidomain protein that localizes to FAs and functions as a scaffold for the recruitment of numerous structural and signaling FA proteins that control cell–ECM adhesion, cytoskeletal organization, and signaling pathways necessary for cell migration and proliferation (Deakin and Turner, 2008). Furthermore, paxillin coordinates the spatiotemporal activation of Rho GTPases, which regulate the actin cytoskeleton, by recruiting GTPase activator, suppressor, and effector proteins to FAs (Deakin and Turner, 2008). Binding partners to paxillin include vinculin, tubulin, and FAK. Furthermore, paxillin localizes to FAs independently of actomyosin contractility and substrate stiffness (Pasapera *et al.*, 2010).

In this study, we examined how substrate stiffness and cytoskeletal tension regulate the relationship between force transmission and vinculin–paxillin recruitment at single FAs. Substrate stiffness and contractility regulate vinculin localization to FAs, and vinculin autoinhibition overrides these effects. Vinculin and paxillin FA area did not correlate with traction force magnitude at single FAs, and this was consistent across different ECM stiffness and cytoskeleton tension states. Vinculin residence time at FAs linearly varied with applied force for stiff substrates, but this coupling was disrupted on soft substrates and in the presence of contractility inhibitors. In contrast, paxillin residence time at FAs was independent of force, substrate stiffness, and cytoskeletal tension. Finally, substrate stiffness and cytoskeletal tension regulate whether vinculin and paxillin turnover dynamics are correlated with each other at single FAs.

RESULTS

Vinculin, but not paxillin, recruitment to FAs depends on substrate stiffness and actomyosin contractility

We first analyzed the effects of substrate stiffness and cytoskeletal contractility on vinculin and paxillin localization to single FAs. We used mouse embryonic fibroblasts (MEFs) expressing fluorescent FA proteins. We chose to use MEFs because they are a commonly used cell type for adhesion studies and generate robust FAs and forces (Dumbauld *et al.*, 2013). Vinculin-null MEFs expressing enhanced green fluorescent protein (eGFP)–vinculin were lentivirally transduced to express Tag red fluorescent protein (TagRFP)–paxillin. Cells were cultured overnight on micropillar array detectors (mPADs) coated with fibronectin. This platform allows for measurement of cell traction forces by tracking the deflections of micropillars (Tan *et al.*, 2003; Sniadecki and Chen, 2007; Yang *et al.*, 2011). We used mPADs presenting a range of substrate stiffness values. The effective substrate stiffness of mPADs was modulated by changing micropost heights, where increasing the post height decreased the effective substrate stiffness (Yang *et al.*, 2011).

We found that substrate stiffness significantly influences the recruitment of vinculin to FAs, consistent with previous work (Pasapera *et al.*, 2010). There was poor localization of vinculin to FAs on 3-kPa mPADs (Figure 1A). Vinculin showed improved localization to FAs on 5- and 14-kPa mPADs (Figure 1A). We observed significant paxillin localization to FAs for substrates with different stiffness (3, 5, and 14 kPa; Figure 1B). Vinculin FA area increased on stiffer substrates (Figure 1C). In contrast, paxillin area at FAs was independent of substrate stiffness (Figure 1D). These results demonstrate that substrate stiffness significantly regulates vinculin, but not paxillin, localization to FAs. These observations are limited to this substrate stiffness range because 3 kPa is the softest mPAD that can be currently prepared.

We next examined the effects of actomyosin contractility on vinculin and paxillin localization to FAs on fibronectin-coated mPADs. Treatment with blebbistatin (20 μM, 1 h), a potent and selective inhibitor of myosin II activity (Kovacs *et al.*, 2004), significantly reduced vinculin localization to FAs and vinculin area at FAs for 5- and 14-kPa substrates (Figure 1, A and E). Although paxillin localization to FAs was evident in the presence of blebbistatin (Figure 1B), inhibition of contractility did reduce paxillin area at FAs for 3- and 5-kPa substrates (Figure 1F). In contrast to vinculin, blebbistatin treatment had no effect on paxillin FA area for the stiff, 14-kPa substrate (Figure 1F).

The images in Figure 1, A and B, show good colocalization of vinculin and paxillin to FAs, especially for stiffer substrates. We therefore computed the ratio of vinculin intensity to paxillin intensity at single FAs. This intensity ratio was previously used as a metric to compare vinculin and paxillin colocalization to FAs (Yamashita *et al.*, 2014). The vinculin-to-paxillin ratio increased with substrate stiffness, indicating increased colocalization of vinculin and paxillin (Figure 1G). Blebbistatin treatment eliminated the substrate

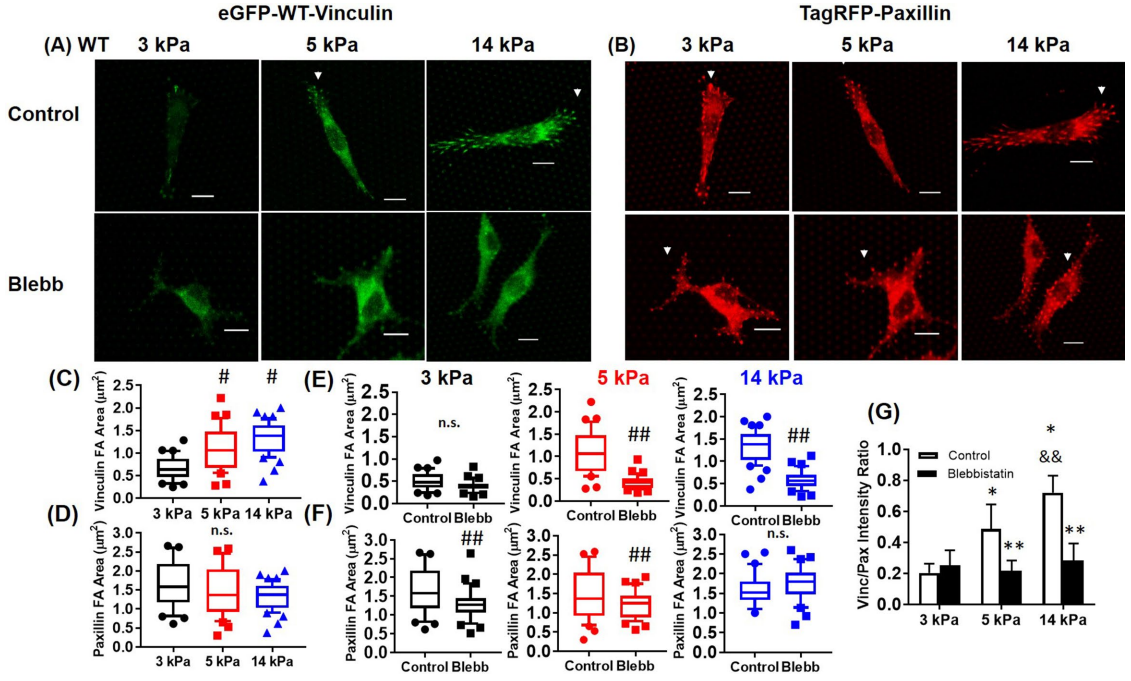

FIGURE 1: WT vinculin recruitment, but not paxillin recruitment, depends on substrate stiffness and cytoskeletal tension. (A) Vinculin (green) and (B) paxillin (red) on mPADs of 3, 5, and 14 kPa in the presence or absence of 20 μM blebbistatin for 1 h. White arrowheads, indicate FAs. Scale bar, 10 μm. Effects of substrate stiffness (C, D) and blebbistatin treatment (E, F) on vinculin and paxillin FA area plotted as box-whisker plots (median and 10th, 25th, 75th, and 90th percentiles; $n > 25$). For WT vinculin FA area, $p < 0.01$ for one-way ANOVA for substrate stiffness. $^{\#}p < 0.01$ vs. 3 kPa, $^{\#\#}p < 0.05$ control vs. blebbistatin. (G) Effects of substrate stiffness and actomyosin contractility on vinculin/paxillin intensity ratio at single FAs ($n > 25$; mean ± SD). $^{*}p < 0.01$ vs. 3 kPa, $^{**}p < 0.01$ vs. respective WT control, and $^{\&\&}p < 0.01$ vs. 5-kPa WT control.

stiffness–dependent increases in vinculin-to-paxillin ratio, demonstrating that actomyosin contractility is required for vinculin-paxillin colocalization to FAs.

Vinculin autoinhibition is crucial to FA localization and overrides the effects of cytoskeletal contractility and substrate stiffness

Chen *et al.* (2006) showed that simultaneous vinculin-head binding to talin and vinculin-tail binding to the actin cytoskeleton promotes vinculin activation and FA localization. However, this model has not been tested as a function of both substrate stiffness and cytoskeletal contractility. Therefore we sought to determine the role of vinculin's autoinhibition in FA localization and whether this depended on substrate stiffness or cytoskeletal tension. We used a MEF line that expresses eGFP–T12 vinculin (Dumbauld *et al.*, 2013). The T12 vinculin mutant is a full-length variant with mutations on the head–tail interface that reduce head-to-tail binding affinity by 100-fold, resulting in an open conformation that can readily bind actin and talin (Cohen *et al.*, 2005). We also lentivirally transduced the eGFP–T12 vinculin MEFs to express TagRFP-paxillin to assess the colocalization between T12 vinculin and paxillin.

We observed significant localization of both T12 vinculin and paxillin to FAs on soft (3 kPa), moderate (5 kPa), and stiff (14 kPa) mPAD substrates (Figure 2, A and B). Both T12 vinculin and paxillin area at FAs were independent of substrate stiffness (Figure 2, C and D). Although we still observed significant vinculin and paxillin localization at FAs, blebbistatin treatment significantly decreased vinculin and paxillin area at FAs for 3- and 5-kPa substrates but not for stiffer 14-kPa mPADs (Figure 2, E and F).

We also measured the ratio between T12 vinculin intensity and paxillin intensity at FAs and found that the intensity ratio was high and equivalent across different substrate stiffness and cytoskeletal contractility states (Figure 2G). This result indicates that T12 vinculin and paxillin colocalization to FAs is independent of substrate stiffness and actomyosin contractility. Taken together, our results demonstrate that substrate stiffness and contractility regulate vinculin localization to FAs, and vinculin autoinhibition is a crucial regulatory step in this process, which overrides the effects of cytoskeletal tension and substrate stiffness. This observation is consistent with the previous observation that T12 vinculin FA localization is insensitive to actomyosin contractility (Carisey *et al.*, 2013; Atherton *et al.*, 2015). In contrast to vinculin, paxillin localization to FAs was insensitive to substrate stiffness and actomyosin contractility and independent of vinculin head-tail autoinhibition.

Coupling between force transmission and vinculin–paxillin localization at single FAs

A key advantage of mPADs is the ability to analyze traction force at single FAs for different substrate stiffness values. Although previous studies explored the effects of vinculin's head-tail interactions in driving FA localization (Cohen *et al.*, 2006), it is not fully understood how this process is related to force at the single-FA level. Therefore we used mPADs to measure traction forces for MEFs expressing either wild type (WT) or T12 eGFP-vinculin. Traction forces were computed by measuring micropost deflections and multiplying the deflections by known micropost stiffnesses (Fu *et al.*, 2010; Dumbauld *et al.*, 2013). This allows for simple quantification of forces compared with polyacrylamide gel traction force measurements, which often require

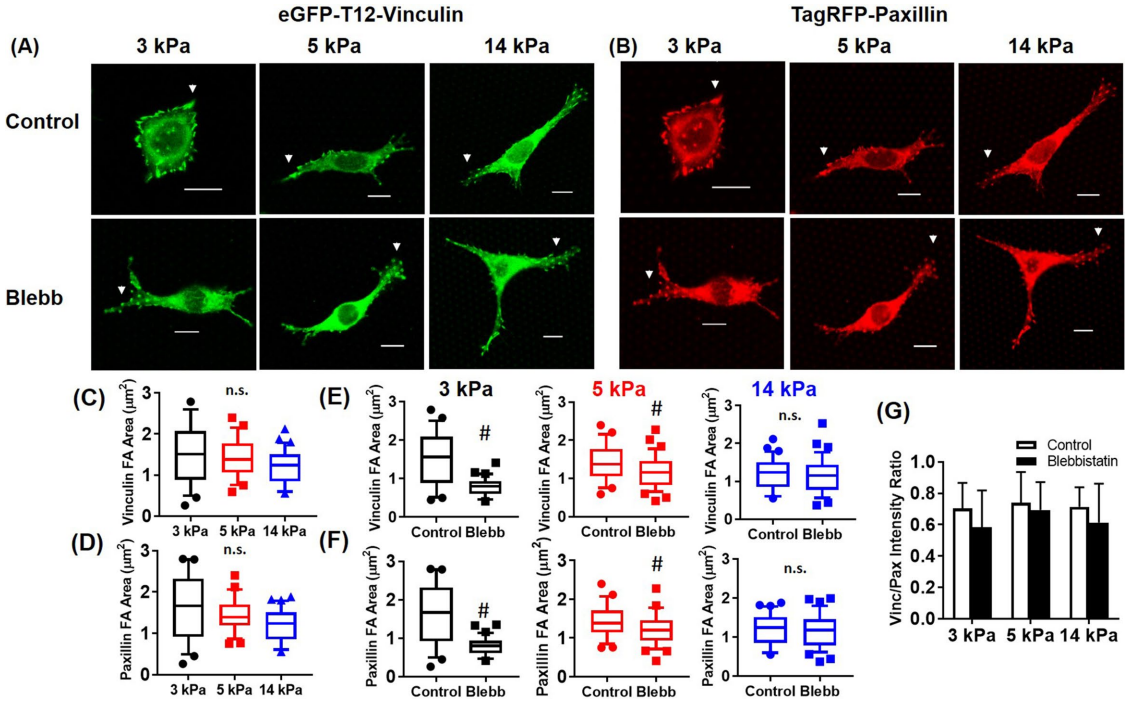

FIGURE 2: T12 vinculin and paxillin recruitment to FAs is independent of substrate stiffness and actomyosin contractility. (A) T12 vinculin (green) and (B) WT paxillin (red) on mPADs of 3, 5, and 14 kPa in the presence or absence of 20 μM blebbistatin for 1 h. White arrowheads indicate FAs. Scale bar, 10 μm. Effects of substrate stiffness (C, D) and blebbistatin treatment (E, F) on T12 vinculin and paxillin FA area plotted as box-whisker plots (median and 10th, 25th, 75th, and 90th percentiles; $n > 25$). $^{\#}p < 0.01$ control vs. blebbistatin. (G) Effects of substrate stiffness and actomyosin contractility on T12 vinculin/paxillin ratio at single FAs ($n > 25$; mean ± SD).

sophisticated computer algorithms (Sabass *et al.*, 2008). We analyzed forces at single FAs on 3-, 5-, and 14-kPa mPADs with or without blebbistatin treatment. WT vinculin–expressing MEFs exhibited significantly higher forces at single FAs on 14-kPa mPADs than with cells cultured on a 3- or 5-kPa substrate (Figure 3A). Blebbistatin treatment (20 μM, 1 h) significantly reduced forces at single FAs for all substrate stiffness values evaluated. We next analyzed the relationship between traction force and vinculin or paxillin area at single FAs. Consistent with previous reports (Stricker *et al.*, 2011; Oakes and Gardel, 2014), we found that vinculin or paxillin area did not correlate with traction force at the single-FA level (Figure 3, B and C). In addition, this was consistent across different stiffness values, even though vinculin FA area varied significantly, depending on the stiffness value analyzed, whereas paxillin FA area was largely independent of stiffness (Figure 3). We observed similar results, albeit with lower traction forces, for MEFs treated with blebbistatin on 3-, 5-, and 14-kPa mPADs as well (Figure 3, B and C, and Supplemental Table S1).

We repeated this analysis for MEFs expressing T12 vinculin and observed similar results, in which T12 vinculin-expressing cells displayed higher forces at FAs on stiffer substrates (Figure 4A). Furthermore, blebbistatin treatment significantly reduced forces at FAs on all stiffness values (Figure 4A). T12 vinculin or paxillin FA area correlated poorly with traction force at the single-FA level for all substrate stiffness values examined and in the presence of blebbistatin (Figure 4, B and C). Stricker *et al.* (2011) reported that without knowledge of FA assembly history, FA size is a poor predictor of the degree of tension exerted on the ECM. Here we extend these findings for both vinculin and paxillin for varying substrate stiffness and cytoskeletal tension states.

Effects of substrate stiffness on vinculin and paxillin residence time at FAs

FA turnover rate regulates cell migration and spreading (Webb *et al.*, 2002; Wolfenson *et al.*, 2011). Furthermore, FAs function as sites for stiffness mechanosensing and force transmission (Balaban *et al.*, 2001; Tan *et al.*, 2003; Dumbauld *et al.*, 2013; Case *et al.*, 2015). Although others have analyzed turnover of different FA proteins and whether cytoskeletal contractility modulates FA turnover rates (Wolfenson *et al.*, 2011), most of these studies have been performed on glass substrates, with mechanical properties that poorly represent physiological values. Furthermore, how force is related to FA turnover is poorly understood. We previously reported a model of vinculin turnover at FAs in which forces applied across the vinculin molecule increase vinculin's residence time at FAs (Dumbauld *et al.*, 2013). We therefore sought to examine the relationship between traction force and vinculin–paxillin turnover at single FAs in the context of substrate stiffness and cytoskeletal contractility.

We examined the relationship between vinculin and paxillin residence times at FAs and applied force by performing fluorescence recovery after photobleaching (FRAP) experiments on cells on mPADs of different stiffness values. We examined recovery times after photobleaching for eGFP-vinculin– and TagRFP-paxillin–containing FAs associated with posts with known deflections. In this manner, we were able to monitor vinculin dynamics at FAs under force. Figure 5 demonstrates representative recovery images and profiles for both vinculin and paxillin under varying levels of traction force.

First, we analyzed the effects of substrate stiffness on vinculin and paxillin turnover at single FAs on 5-, 9-, 14-, and 17-kPa mPADs (Figure 6). We did not include 3-kPa mPADs for the FRAP studies

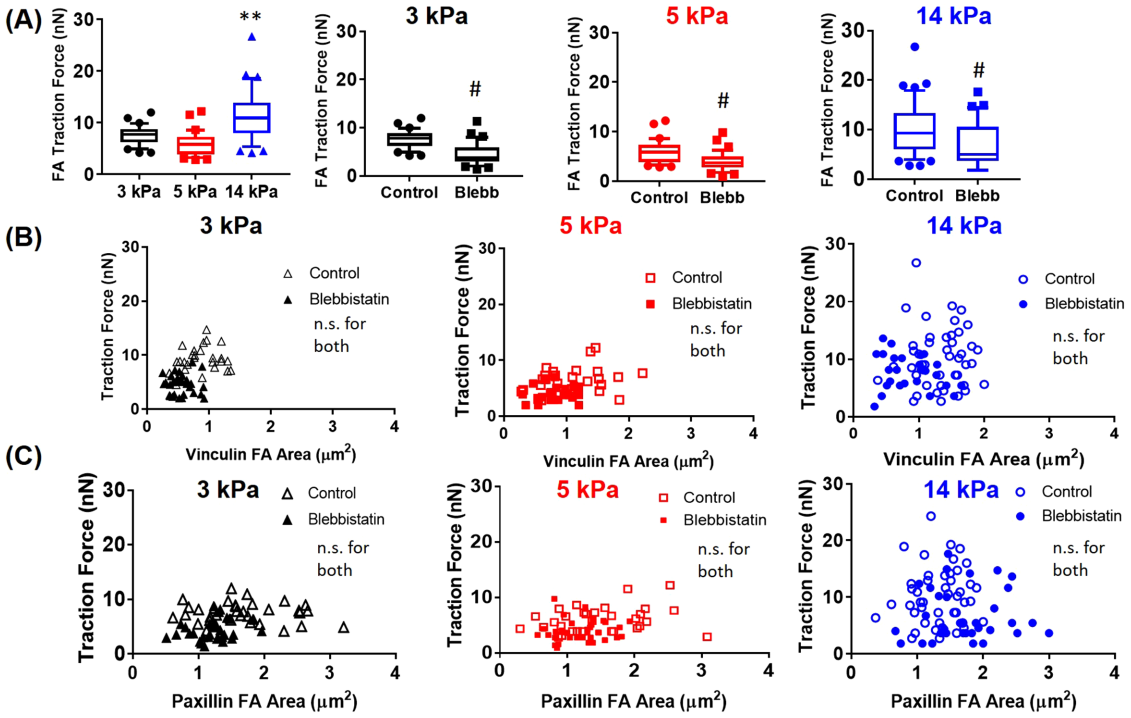

FIGURE 3: Traction forces at single FAs for MEFs expressing WT vinculin and WT paxillin in the presence or absence of blebbistatin. (A) Traction forces at single FAs for WT MEFs cultured on mPADs of 3, 5, and 14 kPa ($n > 25$ FAs, randomly selected from six cells on each condition). $p < 0.01$ for one-way ANOVA, $^{**}p < 0.01$ vs. 3 and 5 kPa, $^{\#}p < 0.01$ vs. blebbistatin. (B, C) Relationship between traction force and FA area at single FAs.

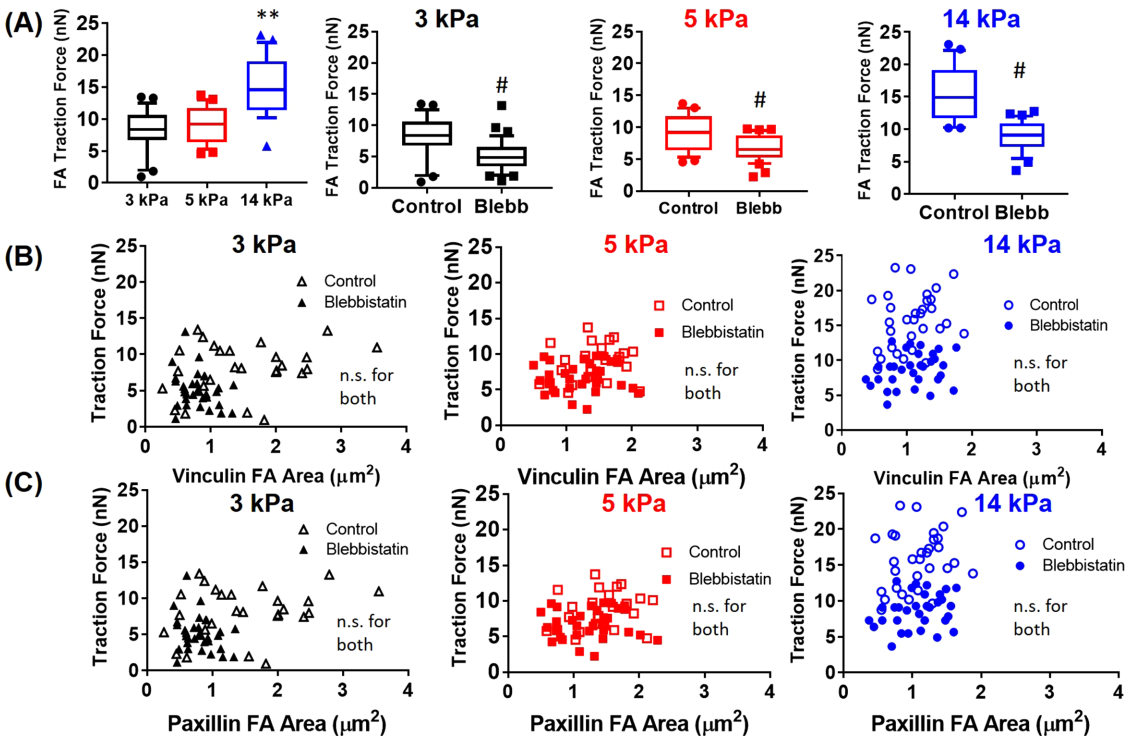

FIGURE 4: Traction forces at single FAs for MEFs expressing T12 vinculin and WT paxillin in the presence or absence of blebbistatin. (A) Traction forces for T12 MEFs cultured on mPADs of 3, 5, and 14 kPa ($n > 25$ FAs, randomly selected from six cells for each condition). $p < 0.01$ for one-way ANOVA, $^{**}p < 0.01$ vs. 3 and 5 kPa, $^{\#}p < 0.01$ vs. blebbistatin. (B, C) Relationship between traction force and FA area at single FAs.

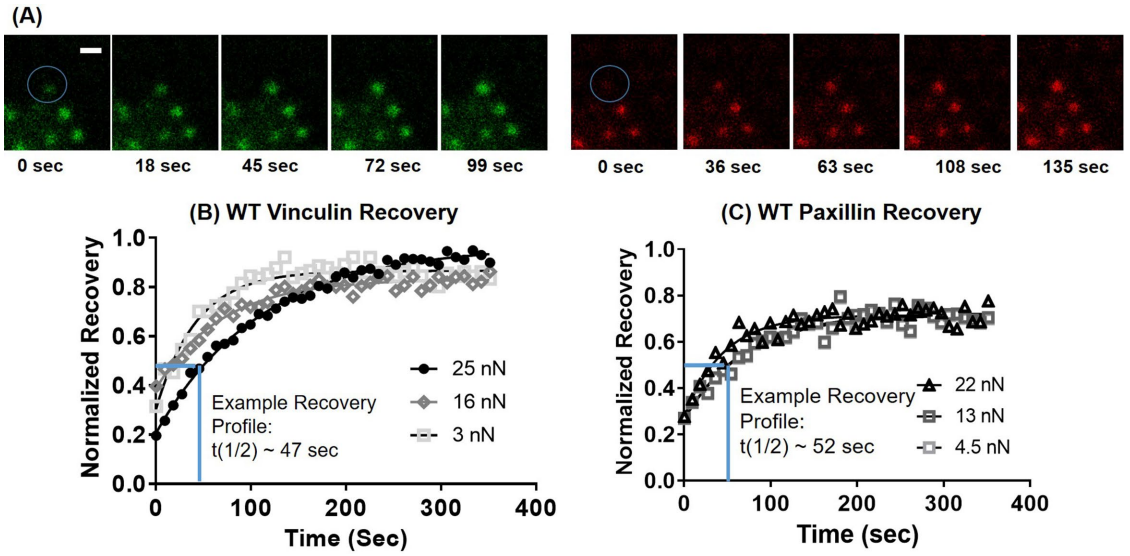

FIGURE 5: FRAP at single FAs. (A) Sample recovery images for vinculin (green) and paxillin (red) for an FA under high (24 nN) force. Scale bar, 4 μm. Blue circle indicates photobleached region. FRAP recovery curves for (B) WT vinculin and (C) WT paxillin recovery at FAs transmitting different forces.

because WT vinculin recruitment to FAs was significantly attenuated on this substrate (Figure 1), making it challenging to reliably photobleach vinculin at FAs. To quantify turnover, our primary metric was the half-life recovery time ($t_{1/2}$), the time it takes for 50% FRAP.

For WT vinculin, vinculin turnover rate at FAs was relatively insensitive to substrate stiffness, although vinculin $t_{1/2}$ on 17-kPa mPADs (~30 s) was significantly lower than that of 5-kPa mPADs (~58 s; Figure 6A). However, linear regression analyses for vinculin $t_{1/2}$ and substrate stiffness showed no relationship (Supplemental Figure S1). We then tested whether cytoskeletal contractility influenced vinculin turnover rate and whether this depended on substrate stiffness. To inhibit contractility, we used Y27632, a potent and selective ROCK inhibitor (Narumiya *et al.*, 2000), because blebbistatin exhibits phototoxicity effects during live-cell imaging (Kolega, 2004). Y-27632 and blebbistatin have similar effects on vinculin–paxillin localization and traction force generation at FAs (Supplemental Figure S2). For WT vinculin, contractility inhibition by Y27632 (10 μM, 30 min) did not alter vinculin turnover rate at FAs for 5-, 9-, 14-, and 17-kPa mPADs (Figure 6B). These results indicate that substrate stiffness and cytoskeletal contractility state do not significantly influence vinculin residence times at single FAs.

We performed similar analyses for paxillin turnover rate at FAs. Substrate stiffness had modest effects on paxillin residence time (Figure 6C). Paxillin $t_{1/2}$ values on 14-kPa substrates (~46 s) were higher than with 5-, 9-, and 17-kPa mPADs (~34 s) but only by 25%. Linear regression analyses showed no relationship between paxillin

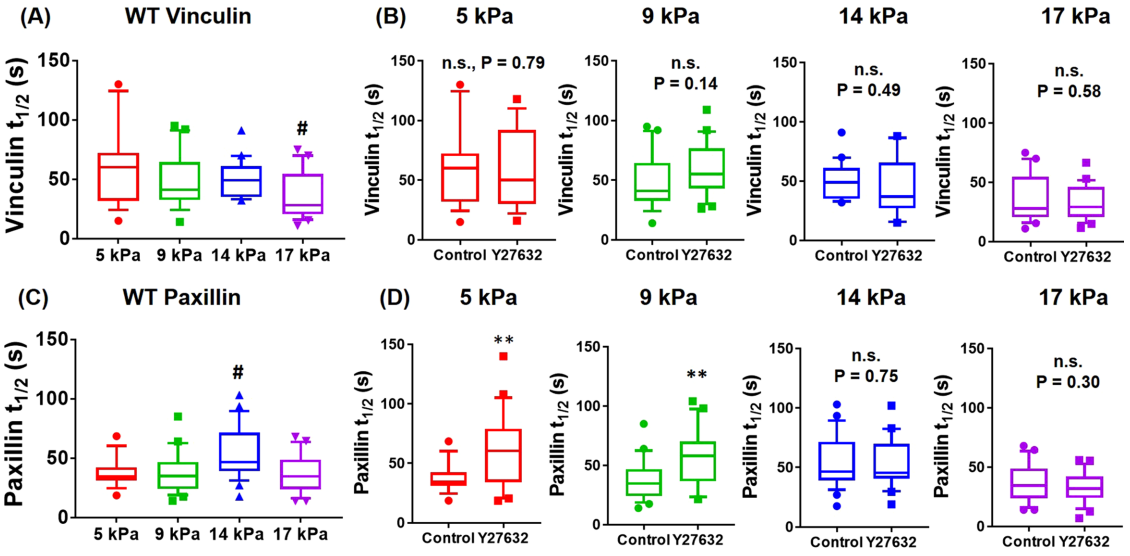

FIGURE 6: Effects of substrate stiffness on (A, B) vinculin and (C, D) paxillin residence times at single FAs plotted as box-whisker plots (median abd10th, 25th, 75th, and 90th percentiles; $n = 18–25$ FAs for each condition). For both vinculin and paxillin, $p < 0.01$ for one-way ANOVA for substrate stiffness. For WT vinculin, $^{\#}p < 0.01$ vs. 5 kPa. For paxillin, $^{\#}p < 0.05$ vs. 5, 9, and 17 kPa, $^{**}p < 0.01$ control vs. Y27632.

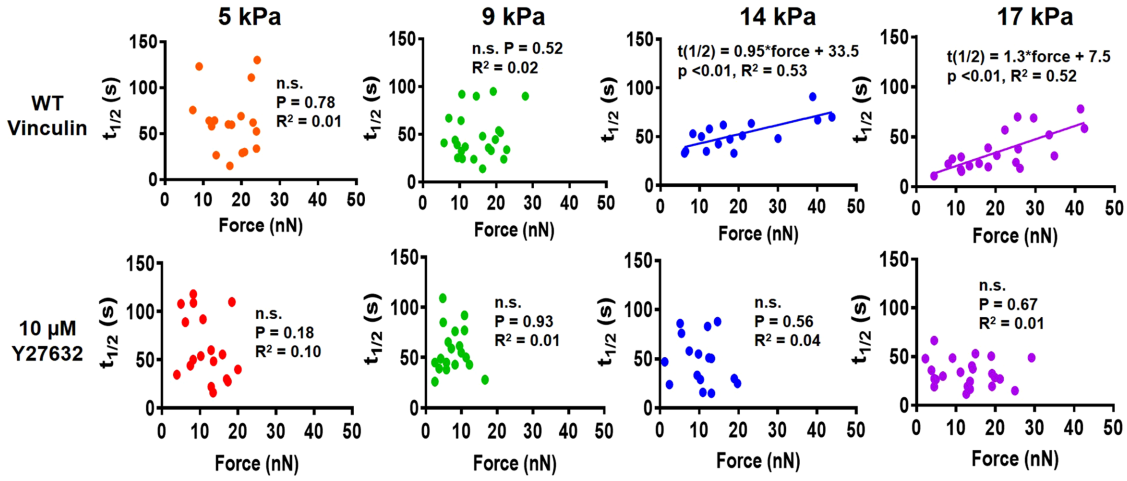

FIGURE 7: Relationship between vinculin $t_{1/2}$ and force at single FAs for MEFs cultured on different substrate stiffness values with and without Y27632 treatment. Vinculin $t_{1/2}$ and force are linearly correlated on 14 and 17 kPa, whereas this correlation is abrogated on softer substrates and after Y27632 treatment.

residence time and substrate stiffness (Supplemental Figure S1). Y27632 treatment (10 μM, 30 min) resulted in higher paxillin $t_{1/2}$ for 5- and 9-kPa substrates but had no effects on stiffer substrates (Figure 6D). These results indicate that paxillin residence time at FAs depends on cytoskeletal tension, but only for soft substrates.

Correlation between force transmission and vinculin–paxillin turnover at FAs

We next examined the relationship between vinculin–paxillin turnover rate and applied traction force at single FAs for different substrate stiffness values. We observed a linear relationship between applied traction force and residence time at FAs for WT vinculin for stiffer mPADs of 14 and 17 kPa (Figure 7). This linear relationship was abrogated on softer mPADs of 5 and 9 kPa. Furthermore, Y27632 eliminated the linear relationship between recovery time and force for vinculin on stiff mPADs of 14 and 17 kPa. These findings support a mechanosensitive model for vinculin activation in which forces applied across vinculin maintain the molecule in active conformation to increase residence times at FAs to transfer force under stiffer substrates. However, this relationship holds only on stiff substrates and in the presence of sufficient cytoskeletal contractility. In contrast to vinculin, paxillin residence times at FAs did not vary with applied traction force for any substrate stiffness (Figure 8). Taken together, these data indicate that substrate stiffness and actomyosin regulate the coupling between vinculin turnover rate and local traction force at single FAs, but there is no coupling between paxillin residence time and applied force, substrate stiffness, or cytoskeletal contractility.

Simultaneous measurement of vinculin and paxillin turnover rates at single FAs

The differences between vinculin and paxillin on the dependence of turnover rate on traction force and substrate stiffness prompted us to compare their residence times at the same FA under a given applied traction force. On stiff 14- and 17-kPa mPADs, where we observed linear coupling between vinculin residence time and force,

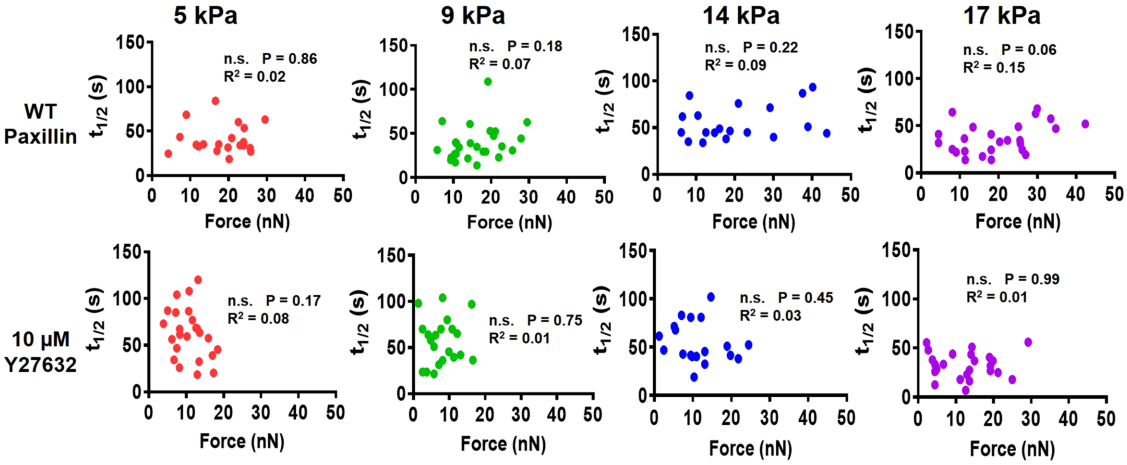

FIGURE 8: Correlation between paxillin $t_{1/2}$ and force at single FAs for MEFs cultured at different substrate stiffness values with or without Y27632 treatment. Paxillin $t_{1/2}$ and force are not correlated at any stiffness values. Furthermore, paxillin $t_{1/2}$ and force are not correlated in the presence or absence of Y27632.

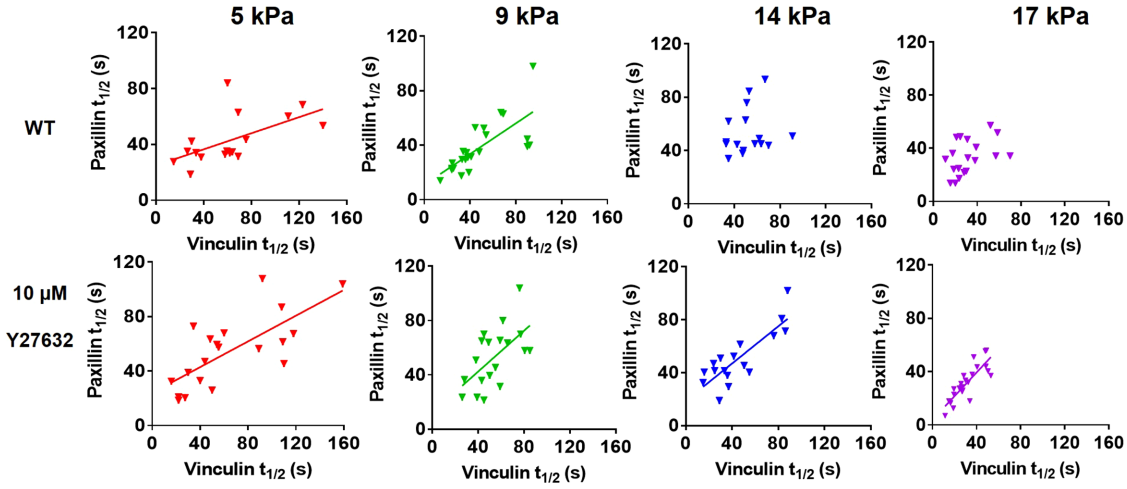

Stiffness	Y27632	Slope ± SE	R^2	P-value vs. Zero Slope	t-test for Y27632
5 kPa	Control	0.288 ± 0.103	0.35	P < 0.05	
5 kPa	Treatment	0.472 ± 0.107	0.52	P < 0.01	n.s. to control
9 kPa	Control	0.563 ± 0.117	0.53	P < 0.01	
9 kPa	Treatment	0.752 ± 0.247	0.36	P < 0.01	n.s. to control
14 kPa	Control	N/A	0.04	n.s. (P = 0.45)	
14 kPa	Treatment	0.704 ± 0.122	0.69	P < 0.01	N/A
17 kPa	Control	N/A	0.19	n.s. (P = 0.06)	
17 kPa	Treatment	0.889 ± 0.129	0.69	P < 0.01	N/A

FIGURE 9: Correlation between vinculin $t_{1/2}$ and paxillin $t_{1/2}$ at single FAs for MEFs cultured at different substrate stiffness values with or without 10 μM Y27632 treatment. Linear correlation between paxillin $t_{1/2}$ and vinculin $t_{1/2}$ at single FAs was observed for MEFs cultured on 5- and 9-kPa substrates and/or after treatment with Y27632.

there was no significant relationship between vinculin and paxillin residence time (Figure 9). However, on softer, 5- and 9-kPa mPADs, a linear relationship between vinculin residence time and paxillin residence time was observed. Strikingly, Y27632 treatment resulted in a linear relationship between vinculin and paxillin residence times at all mPAD stiffness values (Figure 9). Overall these results show that the presence of soft substrates or contractility inhibition yields a strong correlation between vinculin and paxillin residence times at single FAs. However, on stiffer substrates in the presence of actomyosin contractility, vinculin and paxillin residence times are not correlated.

DISCUSSION

How force regulates FA assembly is poorly understood. In this study, we examined the relationship between traction force and vinculin–paxillin localization to single FAs in the context of substrate stiffness and actomyosin contractility. Substrate stiffness and contractility regulated vinculin localization to FAs, whereas they had minimal effects on paxillin localization to FAs. In contrast to WT vinculin, T12 vinculin localization to FAs was independent of substrate stiffness and cytoskeletal contractility, as consistent with previous reports (Carisey *et al.*, 2013). This result indicates that vinculin autoinhibition is a crucial regulatory step in vinculin localization to FAs and overrides the effects of cytoskeletal tension and substrate stiffness.

We also found that vinculin and paxillin FA area does not correlate with traction force magnitude at a single FA, and this observation is consistent across different ECM stiffness and cytoskeletal tension states. However, vinculin residence time at FAs varied linearly with traction force for stiff substrates, but this coupling was disrupted on soft substrates and in the presence of contractility inhibitors. In contrast, paxillin residence time at FAs was independent of traction force, substrate stiffness, and cytoskeletal contractility. Furthermore, substrate stiffness and cytoskeletal contractility regulate whether vinculin and paxillin turnover dynamics are correlated to each other at single FAs. We showed that vinculin turnover and paxillin turnover at the same FA are linearly correlated with each other on soft substrates (5 and 9 kPa) and also with inhibition of contractility. On stiff substrates (14 and 17 kPa), however, this coupling is disrupted, whereas vinculin residence time and force become linearly correlated. These findings suggest that vinculin functions as a mechanosensor for substrate stiffness, contractility, and traction force by modulating vinculin residence time at Fas, whereas paxillin residence time at FAs is insensitive to these mechanical stimuli.

We previously reported that vinculin residence time at FAs correlates with traction force, supporting a mechanosensitive model in which forces stabilize vinculin's active conformation to promote force transfer (Dumbauld *et al.*, 2013). Expression of T12 vinculin, however, disrupted the relationship between applied force and residence time (Dumbauld *et al.*, 2013), underscoring the importance of head–tail inhibition in regulating vinculin residence time. On the basis of our new data, we propose that vinculin serves a mechanosensor and integrator of forces at FAs via its head–tail autoinhibition. At FAs, ECM–integrin traction forces must be balanced by cytoskeletal tension arising from actomyosin contractility for mechanical equilibrium (Coyer *et al.*, 2012). Vinculin regulates this force balance by localizing to FAs and transferring forces across the ECM–cytoskeleton linkage (Dumbauld *et al.*, 2013). Figure 10 presents a conceptual model that captures experimental results for perturbations of the ECM–cytoskeleton force balance.

Substrate stiffness

On stiff substrates, cells generate high traction forces, which are balanced by the high cytoskeletal tension that is necessary for spreading. This results in high forces across the FAs, but if the cytoskeletal tension is too high, the adhesive cluster will detach (Coyer *et al.*, 2012). Because vinculin residence time at FAs varies linearly with traction force on stiff substrates, these elevated forces result in longer vinculin residence times and, consequently, larger vinculin FA area. The increased FA area distributes the applied force across the

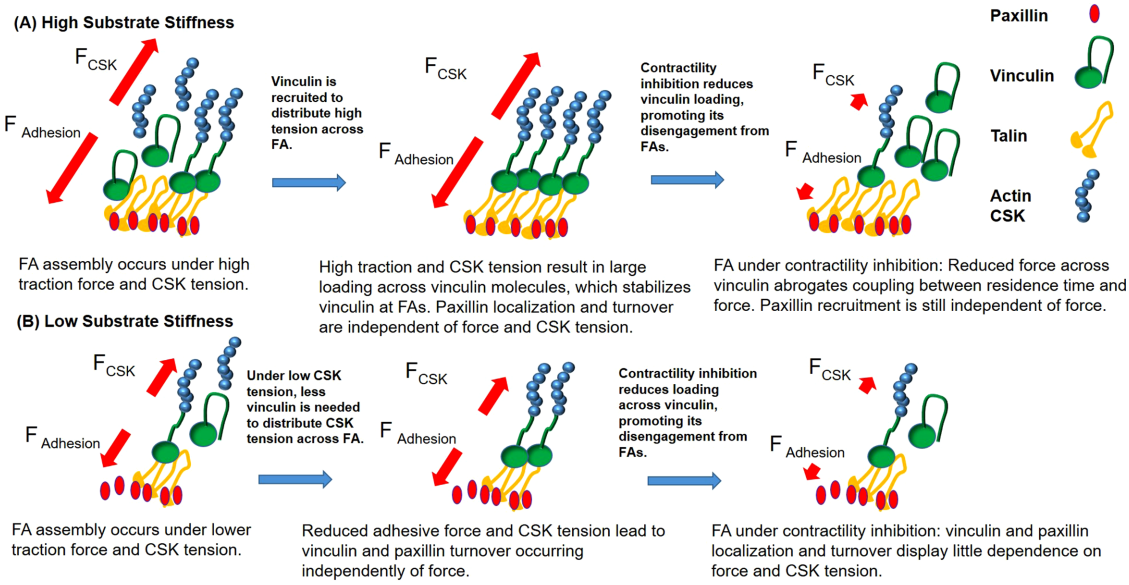

FIGURE 10: Vinculin recruitment depends on a balance between integrin–ECM and cytoskeletal forces at different substrate stiffness values. (A) On stiff substrates, vinculin is recruited to better distribute high applied forces across FAs. High forces applied across vinculin stabilize vinculin at FAs to promote force transfer. Contractility inhibition unloads vinculin molecules and promotes disengagement from FAs. Paxillin recruitment is independent of stiffness and cytoskeletal (CSK) tension. (B) On soft substrates, less vinculin is recruited because there is less force to distribute across FAs. Consequently vinculin recruitment occurs through force-independent mechanisms. Contractility inhibition unloads vinculin molecules and promotes disengagement from FA, whereas paxillin recruitment is largely independent of stiffness and CSK tension.

FA to reduce the load for each ECM–cytoskeletal linkage and prevent the linkages from failing. Conversely, on soft substrates, low traction forces are balanced by low cytoskeletal tension, and therefore low forces are transmitted across the FA. Accordingly, vinculin molecules at the FA carry lower forces, and vinculin residence time at FAs is dominated by other factors, such as head–tail autoinhibition and accessibility to talin-binding domains, which is also reduced on lower loading (del Rio *et al.*, 2009). Indeed, this is consistent with recent work showing that increases in substrate stiffness promote talin's ability to unfold and bind vinculin to promote force transmission (Elosegui-Artola *et al.*, 2016).

Contractility inhibition

Treatment with blebbistatin or Y-27632 inhibits actomyosin contractility to reduce cytoskeletal tension and lower traction forces. The reduced cytoskeletal tension yields lower force transmission across vinculin molecules at the FA. For these lower forces, vinculin turnover is regulated by alternative mechanisms, such as vinculin autoinhibition, as well as by accessibility to talin-binding domains (del Rio *et al.*, 2009). This is consistent with our observation that under contractility inhibition, vinculin turnover is independent of traction force generation at single FAs (Figure 7).

Furthermore, we observed that on soft substrates or in the presence of contractility inhibitors, vinculin and paxillin residence times are correlated with each other. Although the mechanisms driving FA turnover have yet to be fully elucidated, it is clear that actomyosin contractility and substrate stiffness regulate FA activity. Our data suggest that on soft substrates or upon contractility inhibition, vinculin experiences significantly lower forces, and its turnover rate becomes independent of local applied force (Figure 7). We posit that reduced loading forces reduce vinculin activation at FAs, and, consequently, vinculin turnover begins to occur through force-independent mechanisms that may resemble those of paxillin. Indeed, this is consistent with the recent observation that inactive vinculin associates with the lower integrin signaling layer by binding to paxillin, whereas active vinculin associates with the upper force transduction layer by binding to talin and actin (Case *et al.*, 2015).

In contrast to vinculin, paxillin localization to FAs is relatively insensitive to substrate stiffness or actomyosin contractility. We observed significant paxillin localization to FAs for all substrate stiffness values and cytoskeletal tension states. Of interest, we observed that on soft substrates, paxillin recruitment (Figure 1) and turnover (Figure 6) at FAs were both sensitive to actomyosin contractility. In contrast, paxillin recruitment (Figure 1) and turnover (Figure 6) at FAs were insensitive to actomyosin contractility on stiff substrates. The specific mechanisms that govern paxillin recruitment to focal adhesions remain poorly understood. However, it has been proposed that focal FA turnover and recruitment might be influenced by the number of binding partners available (Lele *et al.*, 2008). Reduced substrate stiffness attenuates FAK and vinculin recruitment to FAs, which also serve as binding partners to paxillin (Pasapera *et al.*, 2010). Consequently the altered composition of FAs on softer substrates may affect paxillin recruitment to FAs.

Force and paxillin residence time were independent for all of the substrate stiffness values evaluated. These findings are consistent with the fact that paxillin has not been implicated as a regulator of force transmission at FAs but instead is an important component of the integrin signaling layer (Kanchanawong *et al.*, 2010). Paxillin, however, might still have important functions for mechanotransduction at FAs. For instance, phospho-paxillin facilitates vinculin recruitment to FAs (Pasapera *et al.*, 2010), and FAK-phospho-paxillin-vinculin signaling has been implicated in stiffness sensing during cell migration (Plotnikov *et al.*, 2012).

Taken together, the present results give new insights into the coupling among traction force, substrate stiffness, and FA dynamics.

MATERIALS AND METHODS

Cells and reagents

eGFP–WT vinculin and eGFP–T12 vinculin MEFs have been described previously (Dumbauld *et al.*, 2013). MEFs were lentivirally transduced to express TagRFP-paxillin using EMD Millipore's LentiBrite system. After transduction, TagRFP-paxillin–positive cell populations were enriched by fluorescence-activated cell sorting. Cells were maintained in DMEM containing 10% fetal bovine serum, 1% sodium pyruvate, and 1% penicillin/streptomycin.

Traction force microscopy

The mPAD device silicon masters were prepared as described previously (Fu *et al.*, 2010). In brief, elastomeric micropost arrays were fabricated using polydimethylsiloxane (PDMS) replica molding. To make microfabricated post array templates, 1:10 PDMS prepolymer was cast on top of silanized mPAD device silicon masters, cured at 110°C for 30 min, peeled off gently, oxidized with oxygen plasma (Plasma-Preen; Terra Universal), and silanized overnight with (tridecafluoro-1,1,2,2-tetrahydrooctyl)-1-trichlorosilane (Sigma-Aldrich) vapor under vacuum. To make the final PDMS mPAD device, 1:10 PDMS prepolymer was cast on the template, degassed under vacuum for 20 min, and cured at 110°C for 20 h and gently peeled off the template on a 25-mm-diameter #1 circular coverslip (Electron Microscopy Services). Peeling-induced collapse of the mPADs was rectified by sonication in 100% ethanol, followed by supercritical drying in liquid CO_2 using a critical point dryer (Samdri-PVT-3D; Tousimis). Flat PDMS stamps were generated by casting 1:20 PDMS prepolymer on flat and silanized silicon wafers. Stamps were coated in a saturating concentration of fibronectin (D307, Thermo Fisher; 50 μg/ml in phosphate-buffered saline) for 1 h. These stamps were washed in sterile distilled water and dried under a stream of nitrogen gas. Subsequently fibronectin-coated stamps were placed in contact with surface-oxidized mPAD substrates (UVO-Model 342; Jelight). mPAD substrates were labeled with 5 μg/ml DiD′ (Invitrogen) in distilled water for 10 min. mPAD substrates were subsequently transferred to a solution of 0.2% Pluronics F127 (Sigma-Aldrich) for 30 min to prevent nonspecific protein absorption. MEF cells were seeded in growth medium and then allowed to spread overnight. On the next day, mPAD substrates were transferred to an aluminum coverslip holder (Attofluor Cell Chamber; Invitrogen) for live-cell microscopy and placed in a stage-top incubator that regulated temperature, humidity, and CO_2 (Live Cell; Pathology Devices). Confocal images were taken with a Nikon C2-Confocal Module connected to a Nikon Eclipse Ti inverted microscope, using a high-magnification objective (CFI Plan Apochromat total internal reflection fluorescence [TIRF] 60× oil, numerical aperture [NA] 1.49; Nikon). Post images were captured with a 640-nm laser with a 685/50 filter, vinculin images were captured using a 488-nm laser and 525/50 filter, and paxillin images were captured using a 561-nm laser and 595/50 filter. For force measurements, the top and bottom of the posts were sequentially imaged and the deflection measured. The resulting force, F, was calculated using Euler–Bernoulli beam theory, in which E, D, L, and δ are the Young's modulus, post diameter, post height, and post deflection, respectively:

$$F = \delta \frac{3\pi E D^4}{64 L^3}$$

Fluorescence recovery after photobleaching

A confocal microscope head (Nikon C2) and inverted microscope (Nikon Eclipse Ti) equipped with a Melles-Griot argon 488-nm laser and Coherent Sapphire 561-nm laser under the control of Nikon C2 Elements software were used for FRAP experiments. MEFs expressing eGFP-vinculin and TagRFP-paxillin were seeded overnight on fibronectin-coated mPADs of varying stiffness. Cell-seeded mPADs were loaded into an Attofluor cell chamber (Invitrogen) and allowed to equilibrate for >20 min. A 60× APO TIRF (1.49 N.A.) objective (Nikon) was used for imaging. Initial fluorescence intensity was measured using low laser power (0.3–1.0%) followed by photobleaching of a 0.85-μm-diameter circle inside FAs at 25% laser power (488 nm) and 3.5% (561 nm) laser power for one zoomed pass (bleached circle is defined within 512 × 512 pixel box). The recovery of fluorescence was monitored every 8 s until a plateau in recovery was reached (5 prebleach and 35–40 postbleach images were acquired in each series recorded). Image series were analyzed in Nikon NIS-Elements software, where background subtraction and correction for incidental bleaching during image acquisition were applied to data extracted from the bleached region. Curves were fitted to a single-exponential recovery model by assuming a reaction-dominated system and disregarding any effects of diffusion, and the characteristic recovery time ($t_{1/2}$) was calculated as previously described (Dumbauld *et al.*, 2013).

Statistical analysis

Regression analyses were performed using GraphPad Prism. Analysis of variance (ANOVA), Kruskal–Wallis nonparametric tests, and post hoc tests were performed in GraphPad Prism. $p < 0.05$ was considered significant.

ACKNOWLEDGMENTS

We thank David Dumbauld, Jan Scrimgeour, and Jennifer Curtis for helpful discussions on the FRAP studies. We acknowledge support from National Institutes of Health Grants R01 GM065918 (A.J.G.) and R01 HL127236 (A.J.G.), National Science Foundation Grant CBET 1149401 (J.F.), and a National Science Foundation Graduate Research Fellowship (D.W.Z.) under Grant DGE-1148903.

REFERENCES

Atherton P, Stutchbury B, Wang DY, Jethwa D, Tsang R, Meiler-Rodriguez E, Wang P, Bate N, Zent R, Barsukov IL, *et al.* (2015). Vinculin controls talin engagement with the actomyosin machinery. Nat Commun 6, 10038.

Austen K, Ringer P, Mehlich A, Chrostek-Grashoff A, Kluger C, Klingner C, Sabass B, Zent R, Rief M, Grashoff C (2015). Extracellular rigidity sensing by talin isoform-specific mechanical linkages. Nat Cell Biol 17, 1597–1606.

Balaban NQ, Schwarz US, Riveline D, Goichberg P, Tzur G, Sabanay I, Mahalu D, Safran S, Bershadsky A, Addadi L, Geiger B (2001). Force and focal adhesion assembly: a close relationship studied using elastic micropatterned substrates. Nat Cell Biol 3, 466–472.

Beningo KA, Dembo M, Kaverina I, Small JV, Wang YL (2001). Nascent focal adhesions are responsible for the generation of strong propulsive forces in migrating fibroblasts. J Cell Biol 153, 881–888.

Brindle NP, Holt MR, Davies JE, Price CJ, Critchley DR (1996). The focal-adhesion vasodilator-stimulated phosphoprotein (VASP) binds to the proline-rich domain in vinculin. Biochem J 318, 753–757.

Carisey A, Tsang R, Greiner AM, Nijenhuis N, Heath N, Nazgiewicz A, Kemkemer R, Derby B, Spatz J, Ballestrem C (2013). Vinculin regulates the recruitment and release of core focal adhesion proteins in a force-dependent manner. Curr Biol 23, 271–281.

Case LB, Baird MA, Shtengel G, Campbell SL, Hess HF, Davidson MW, Waterman CM (2015). Molecular mechanism of vinculin activation and nanoscale spatial organization in focal adhesions. Nat Cell Biol 17, 880–892.

Chen H, Choudhury DM, Craig SW (2006). Coincidence of actin filaments and talin is required to activate vinculin. J Biol Chem 281, 40389–40398.
Chen H, Cohen DM, Choudhury DM, Kioka N, Craig SW (2005). Spatial distribution and functional significance of activated vinculin in living cells. J Cell Biol 169, 459–470.
Chrzanowska-Wodnicka M, Burridge K (1996). Rho-stimulated contractility drives the formation of stress fibers and focal adhesions. J Cell Biol 133, 1403–1415.
Cohen DM, Chen H, Johnson RP, Choudhury B, Craig SW (2005). Two distinct head-tail interfaces cooperate to suppress activation of vinculin by talin. J Biol Chem 280, 17109–17117.
Cohen DM, Kutscher B, Chen H, Murphy DB, Craig SW (2006). A conformational switch in vinculin drives formation and dynamics of a talin-vinculin complex at focal adhesions. J Biol Chem 281, 16006–16015.
Coyer SR, Singh A, Dumbauld DW, Calderwood DA, Craig SW, Delamarche E, Garcia AJ (2012). Nanopatterning reveals an ECM area threshold for focal adhesion assembly and force transmission that is regulated by integrin activation and cytoskeleton tension. J Cell Sci 125, 5110–5123.
Deakin NO, Turner CE (2008). Paxillin comes of age. J Cell Sci 121, 2435–2444.
del Rio A, Perez-Jimenez R, Liu R, Roca-Cusachs P, Fernandez JM, Sheetz MP (2009). Stretching single talin rod molecules activates vinculin binding. Science 323, 638–641.
DeMali KA, Barlow CA, Burridge K (2002). Recruitment of the Arp2/3 complex to vinculin: coupling membrane protrusion to matrix adhesion. J Cell Biol 159, 881–891.
Dumbauld DW, Lee TT, Singh A, Scrimgeour J, Gersbach CA, Zamir EA, Fu J, Chen CS, Curtis JE, Craig SW, Garcia AJ (2013). How vinculin regulates force transmission. Proc Natl Acad Sci USA 110, 9788–9793.
Dumbauld DW, Shin H, Gallant ND, Michael KE, Radhakrishna H, Garcia AJ (2010). Contractility modulates cell adhesion strengthening through focal adhesion kinase and assembly of vinculin-containing focal adhesions. J Cell Physiol 223, 746–756.
Elosegui-Artola A, Oria R, Chen Y, Kosmalska A, Perez-Gonzalez C, Castro N, Zhu C, Trepat X, Roca-Cusachs P (2016). Mechanical regulation of a molecular clutch defines force transmission and transduction in response to matrix rigidity. Nat Cell Biol 18, 540–548.
Engler AJ, Sen S, Sweeney HL, Discher DE (2006). Matrix elasticity directs stem cell lineage specification. Cell 126, 677–689.
Fu J, Wang YK, Yang MT, Desai RA, Yu X, Liu Z, Chen CS (2010). Mechanical regulation of cell function with geometrically modulated elastomeric substrates. Nat Methods 7, 733–736.
Giannone G, Dubin-Thaler BJ, Rossier O, Cai Y, Chaga O, Jiang G, Beaver W, Dobereiner HG, Freund Y, Borisy G, Sheetz MP (2007). Lamellipodial actin mechanically links myosin activity with adhesion-site formation. Cell 128, 561–575.
Grashoff C, Hoffman BD, Brenner MD, Zhou R, Parsons M, Yang MT, McLean MA, Sligar SG, Chen CS, Ha T, Schwartz MA (2010). Measuring mechanical tension across vinculin reveals regulation of focal adhesion dynamics. Nature 466, 263–266.
Heisenberg CP, Bellaiche Y (2013). Forces in tissue morphogenesis and patterning. Cell 153, 948–962.
Humphries JD, Byron A, Bass MD, Craig SE, Pinney JW, Knight D, Humphries MJ (2009). Proteomic analysis of integrin-associated complexes identifies RCC2 as a dual regulator of Rac1 and Arf6. Sci Signal 2, ra51.
Humphries JD, Byron A, Humphries MJ (2006). Integrin ligands at a glance. J Cell Sci 119, 3901–3903.
Johnson RP, Craig SW (1995). F-actin binding site masked by the intramolecular association of vinculin head and tail domains. Nature 373, 261–264.
Kanchanawong P, Shtengel G, Pasapera AM, Ramko EB, Davidson MW, Hess HF, Waterman CM (2010). Nanoscale architecture of integrin-based cell adhesions. Nature 468, 580–584.
Kolega J (2004). Phototoxicity and photoinactivation of blebbistatin in UV and visible light. Biochem Biophys Res Commun 320, 1020–1025.
Kovacs M, Toth J, Hetenyi C, Malnasi-Csizmadia A, Sellers JR (2004). Mechanism of blebbistatin inhibition of myosin II. J Biol Chem 279, 35557–35563.
Kuroda M, Wada H, Kimura Y, Ueda K, Kioka N (2017). Vinculin promotes nuclear localization of TAZ to inhibit ECM stiffness-dependent differentiation into adipocytes. J Cell Sci 130, 989–1002.
Lele TP, Thodeti CK, Pendse J, Ingber DE (2008). Investigating complexity of protein-protein interactions in focal adhesions. Biochem Biophys Res Commun 369, 929–934.
Liu Z, Bun P, Auduge N, Coppey-Moisan M, Borghi N (2016). Vinculin head-tail interaction defines multiple early mechanisms for cell substrate rigidity sensing. Integr Biol (Camb) 8, 693–703.
Lo CM, Wang HB, Dembo M, Wang YL (2000). Cell movement is guided by the rigidity of the substrate. Biophys J 79, 144–152.
Mitra SK, Hanson DA, Schlaepfer DD (2005). Focal adhesion kinase: in command and control of cell motility. Nat Rev Mol Cell Biol 6, 56–68.
Narumiya S, Ishizaki T, Uehata M (2000). Use and properties of ROCK-specific inhibitor Y-27632. Methods Enzymol 325, 273–284.
Oakes PW, Gardel ML (2014). Stressing the limits of focal adhesion mechanosensitivity. Curr Opin Cell Biol 30, 68–73.
Palmer SM, Playford MP, Craig SW, Schaller MD, Campbell SL (2009). Lipid binding to the tail domain of vinculin: specificity and the role of the N and C termini. J Biol Chem 284, 7223–7231.
Pasapera AM, Schneider IC, Rericha E, Schlaepfer DD, Waterman CM (2010). Myosin II activity regulates vinculin recruitment to focal adhesions through FAK-mediated paxillin phosphorylation. J Cell Biol 188, 877–890.
Pelham RJ Jr, Wang Y (1997). Cell locomotion and focal adhesions are regulated by substrate flexibility. Proc Natl Acad Sci USA 94, 13661–13665.
Plotnikov SV, Pasapera AM, Sabass B, Waterman CM (2012). Force fluctuations within focal adhesions mediate ECM-rigidity sensing to guide directed cell migration. Cell 151, 1513–1527.
Provenzano PP, Keely PJ (2011). Mechanical signaling through the cytoskeleton regulates cell proliferation by coordinated focal adhesion and Rho GTPase signaling. J Cell Sci 124, 1195–1205.
Sabass B, Gardel ML, Waterman CM, Schwarz US (2008). High resolution traction force microscopy based on experimental and computational advances. Biophys J 94, 207–220.
Sniadecki NJ, Chen CS (2007). Microfabricated silicone elastomeric post arrays for measuring traction forces of adherent cells. Methods Cell Biol 83, 313–328.
Stricker J, Aratyn-Schaus Y, Oakes PW, Gardel ML (2011). Spatiotemporal constraints on the force-dependent growth of focal adhesions. Biophys J 100, 2883–2893.
Subauste MC, Pertz O, Adamson ED, Turner CE, Junger S, Hahn KM (2004). Vinculin modulation of paxillin-FAK interactions regulates ERK to control survival and motility. J Cell Biol 165, 371–381.
Tan JL, Tien J, Pirone DM, Gray DS, Bhadriraju K, Chen CS (2003). Cells lying on a bed of microneedles: an approach to isolate mechanical force. Proc Natl Acad Sci USA 100, 1484–1489.
Webb DJ, Parsons JT, Horwitz AF (2002). Adhesion assembly, disassembly and turnover in migrating cells – over and over and over again. Nat Cell Biol 4, E97–E100.
Weng S, Shao Y, Chen W, Fu J (2016). Mechanosensitive subcellular rheostasis drives emergent single-cell mechanical homeostasis. Nat Mater 15, 961–967.
Wolfenson H, Bershadsky A, Henis YI, Geiger B (2011). Actomyosin-generated tension controls the molecular kinetics of focal adhesions. J Cell Sci 124, 1425–1432.
Yamashita H, Ichikawa T, Matsuyama D, Kimura Y, Ueda K, Craig SW, Harada I, Kioka N (2014). The role of the interaction of the vinculin proline-rich linker region with vinexin alpha in sensing the stiffness of the extracellular matrix. J Cell Sci 127, 1875–1886.
Yang MT, Fu J, Wang YK, Desai RA, Chen CS (2011). Assaying stem cell mechanobiology on microfabricated elastomeric substrates with geometrically modulated rigidity. Nat Protoc 6, 187–213.
Yeung T, Georges PC, Flanagan LA, Marg B, Ortiz M, Funaki M, Zahir N, Ming W, Weaver V, Janmey PA (2005). Effects of substrate stiffness on cell morphology, cytoskeletal structure, and adhesion. Cell Motil Cytoskeleton 60, 24–34.
Ziegler WH, Liddington RC, Critchley DR (2006). The structure and regulation of vinculin. Trends Cell Biol 16, 453–460.